Journal of Agricultural Engineering

Journal of Agricultural Engineering 2026; LVII:1864
doi:10.4081/jae.2026.1864

Investigation on the design and optimization of a high-speed precision maize metering device with a layered centrifugal mechanical structure

Meng Zhang,[1] Xinyu Li,[2] Jin Ma,[2] Lei Wang,[3] Qinghui Lai,[4] Yanchao Yin[1]

[1]Faculty of Mechanical and Electrical Engineering, Kunming University of Science and Technology, Kunming; [2]College of Mechanical and Electronic Engineering, Northwest A&F University, Yangling; [3]College of Engineering, Nanjing Agricultural University, Nanjing; [4]School of Energy and Environment Science, Yunnan Normal University, Kunming, China

Abstract

To meet the requirements of high-speed precision maize seeding, a novel centrifugal mechanical high-speed precision metering device was developed. The device performs seed filling and seed clearing by utilizing the seed pile stratification and the centrifugal force generated during high-speed operation, fundamentally changing the traditional method of seed pile filling to a layered and discrete seed pile arrangement. To identify the optimal performance parameters, an orthogonal rotational combination test was conducted with the rotating speed of the seed metering disc, number of apertures, and aperture diameters as test factors, with quality of feed index, miss index, and multiples index as evaluation indicators, and the relationships between the various factors and evaluation indicators were established. Response surface methodology was used to optimize the results, which were further verified through bench testing. The results indicated that increasing the rotating speed of the metering disc had no significant impact on the quality of feed index, demonstrating the system's suitability for high-speed operation. Under a plant spacing of 180 mm, with a rotating speed of 1729.01 rad/min (approximately 12 km/h), five apertures, and an aperture diameter of 14 mm, the quality of feed index reached 92.07%. Bench testing confirmed the reliability of the optimization results.

Key words: centrifugation; stratification; high-speed precision metering device; maize.

Correspondence: Yanchao Yin, Faculty of Mechanical and Electrical Engineering, Kunming University of Science and Technology, 727 Jingmingnan Rd., Chenggong District, 650500 Kunming, China. E-mail: yinyc@163.com

Introduction

High-speed precision seeding refers to the process in which seeds are accurately placed into the soil at consistent seed spacing, row spacing, and sowing depth, based on the requirements of agronomy, using precision drills with high-speed operational capabilities (more than 10 km/h) (Chen *et al*., 2024; Tang *et al*., 2023). High-performance high-speed precision drills are an effective means to achieve superior seeding quality (Dong *et al*., 2025; Guo *et al*., 2022). These drills can significantly reduce seed usage, minimize field operations, and achieve uniform, strong, and healthy seedlings, thereby lowering costs and increasing yield (Li *et al*., 2024a; Xie *et al*., 2025). As the core component, the performance and adaptability of the high-speed precision metering device play a crucial role in the technology of maize seeding (Anantachar *et al*., 2010; Gao *et al*., 2022).

Precision seed metering devices can be broadly categorized into mechanical metering devices and pneumatic metering devices (Bu *et al*., 2024; Zhao *et al*., 2024). Mechanical metering devices include disc type (Xu *et al*., 2025), cell-wheel type (Chen *et al*., 2022), spoon-wheel type (Li *et al*., 2020), and finger-clamp type devices (Ding *et al*., 2023). Their strengths lie in structural simplicity, ease of manufacturing, and low cost. However, because their seed-filling process mainly depends on gravity or mechanical clamping, it is difficult to achieve effective filling under high-speed conditions (Xiong *et al*., 2021). To effectively address the problem of poor seed filling, current methods adopt mechanical stirring, such as using metering discs with grooves and seed cells with stirring functions or utilizing airflow disturbance and electromagnetic vibration. The main objective is to increase seed flowability and improve filling performance (Nikolay *et al*., 2022; Ospanova *et al*., 2024). Previous studies have primarily adopted gravity-based seed filling with aggregated seed piles and focused on improving seed pile disturbance to address the problem of poor seed flow-ability, which leads to inadequate filling (Tang *et al*., 2022).

Pneumatic metering devices can be classified into central air-assisted system (Lei *et al*., 2018, 2016) or per row unit with each divided further by air-blow or air-suction (Han *et al*., 2018). These types offer advantages such as suitability for high-speed operations, high precision, and minimal seed damage. As a result, their adoption has been steadily increasing (Gao *et al*., 2023; Shang *et al*., 2024). However, pneumatic systems require the addition of an air power unit, making the structure more complex and the cost significantly higher (Wang *et al*., 2017). Moreover, these systems rely primarily on gravity-based seed filling, which performs poorly under high-speed operation especially for maize, whose non-spherical seed shape leads to ineffective filling and a high rate of missed

seeding (Dong *et al*., 2024; Li *et al*., 2024b). However, these approaches have not fundamentally altered the working principles or structural design of the metering devices to resolve the difficulties in seed filling under high-speed operations caused by gravity-based aggregation.

In addition, the existing seed metering devices have room for improvement in seed damage, missed, multiples, and speed. Seed damage refers to the physical damage caused to seeds during the metering process, which can damage germination and seedling emergence. For modern metering devices, the damage rate of fragile seeds may rise to 5-8 % (Li *et al*., 2023). Meanwhile, traditional mechanical meters are often limited to 6-8 km/h to maintain accuracy, while advanced pneumatic systems can operate at 10-12 km/h without significant performance loss. However, speed-related challenges persist above 12 km/h, even state-of-the-art devices may exhibit increased misses (up to 15%) due to inadequate seed filling and release timing (Gao *et al*., 2023).

To address the poor seed-filling performance of mechanical metering devices under high-speed operation, a novel mechanical high-speed precision maize metering device was developed based on a new design concept and structure. The device utilizes seed-disturbing teeth to agitate the seed pile, features a layered and discretized seed pile instead of a static seed pile, and utilizes the centrifugal force generated during high-speed operation to perform both seed filling and seed clearing. The unfavorable conditions originally caused by high-speed operation are transformed into favorable ones, fundamentally resolving the problem of short seed-filling time and poor filling performance under high-speed operation in traditional systems. A second-order regression orthogonal rotation combination experiment was conducted using three key factors influencing seed-filling performance -metering disc rotating speed, aperture numbers, and aperture diameter- as experimental variables. The aim was to provide design references for high-speed precision maize metering devices.

Materials and Methods

Structure and working principle of the metering device

The layered centrifugal mechanical high-speed precision maize metering device is composed of a seed metering disc, seed-protecting plate, seed cells, seed-disturbing teeth, front housing, and seed box, as shown in Figure 1. In addition to the shaft, the other accessories are polyoxymethylene (POM) material 3D printing. When the metering device is in operation, maize seeds accumulate within the chamber of the device. The seed-disturbing teeth stir the seeds, loosening the seed pile and enabling the lower-layer seeds to pass through the apertures on the partition plate into the seed-filling zone, thereby achieving seed pile stratification. In the seed-filling zone, seeds enter the seed cells under the combined effect of gravity and centrifugal force as the metering disc rotates. With the clamping action of the seed cells and the seed-protecting plate, the seeds inside the cells rotate along with the metering disc, passing through the seed-filling and seed-carrying zones and reaching the topmost position of the metering device. At this point, the front-end inclined section of the seed-protecting plate in the seed-filling and seed-carrying arc segments fit closely with the seed cells to assist in seed filling. In the seed-clearing zone, the width of the inclined section narrows, allowing only one seed to remain in each cell. The excess seeds, having lost the supporting force of the seed-protecting plate, are subjected to centrifugal force and are ejected from the cells. These seeds are then guided back through the seed returning pipe to the seed-filling zone for refilling. The single seed remaining in the seed cells continues to rotate along with the cells until it reaches the seed-dropping zone, where the protection of the seed-protecting plate is removed. Lacking supporting force, the seed falls out of the cells under its own weight and is discharged from the metering device through the seed outlet, completing the entire seed metering process, as shown in Figure 2.

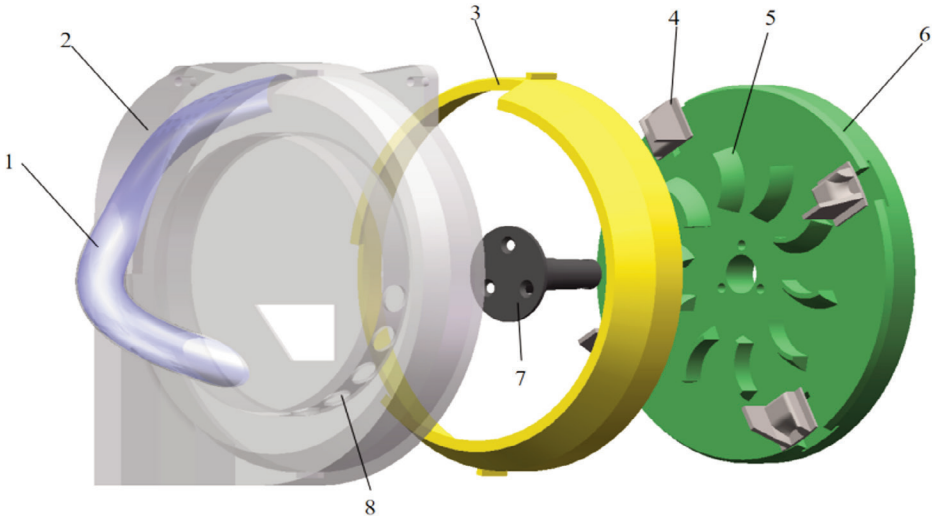

Figure 1. Structure diagram of seed metering device. 1. seed returning pipe; 2. front housing 3. seed-protecting plate; 4. seed cell; 5. seed-disturbing teeth; 6. seed metering disc; 7. shaft; 8. aperture.

Design of key components of the metering device

Design of the seed metering disc

The metering disc provides the necessary supporting force for maize seeds during the seed-carrying process. The structure of the metering device is directly related to its overall size, the linear velocity of the metering disc, and other key parameters. Among these, the seed-filling time is only associated with the arc length of the seed-filling zone and the rotating speed of the metering disc, and is independent of the disc diameter (Chen *et al*., 2024). Currently, the common diameter range of metering discs is between 140 mm and 260 mm. When the disc diameter is large, its linear velocity increases correspondingly, enhancing the centrifugal force acting on the seeds within the seed cells. This increased centrifugal force helps to eject excess seeds from the seed cells in the seed-clearing zone. However, if the diameter is too large, the centrifugal force during high-speed rotation may become excessive, potentially leading to difficulties in seed filling. Considering the seeder's overall size, the diameter of the metering disc is designed to be 200 mm. Additionally, four seed cells are evenly spaced around the outer circumference of the metering disc. These seed cells are designed to accommodate interchangeable seed cells, facilitating the adaptation to different seed shapes and sizes during sowing operations.

The diameter of the metering disc and the number of seed cells directly affect the minimum sowing speed of the metering device. Figure 3 illustrates the forces acting on a maize seed when it rotates to the highest point along with the metering disc, where the radial force on the seed satisfies Eq. (1).

$$F_y = F_c - G - f \quad \text{(Eq. 1)}$$

where: F_y is the radial force acting on the seed (N); G is the gravitational force acting on the seed (N); f is the friction force acting on the seed (N).

When the resultant radial force is greater than zero, the lowermost seed in the seed cell will not be ejected, and the excess seeds entering the seed-clearing zone can be cleared out of the seed cells. The higher the rotating speed of the metering disc, the greater the centrifugal force on the seeds. Therefore, when $F_C = G$, the rotating speed of the metering disc reaches its minimum value. Because the maize seed and the metering disc are rigid and smooth, the surface adhesion is small when the two are in contact, so the friction force is ignored, satisfying Eq. (2).

$$\begin{cases} F_c = G \\ G = mg \\ F_c = \dfrac{mn^2\pi^2 d}{1800} \end{cases} \quad \text{(Eq. 2)}$$

where: g is the gravitational acceleration (m/s²); d is the diameter of the metering disc (mm); n is the rotating speed of the metering disc (rad/min); m is the mass of the seed (kg).

The relationship between the sowing speed and the rotating speed of the metering disc satisfies Eq. (3):

$$v = 0.06nac \quad \text{(Eq. 3)}$$

where: v is forward speed of the seeder (m/s); a is number of seed cells on the metering disc; c is maize plant spacing (mm).

Based on the derived equations, under dense planting conditions (with a maize plant spacing of 180 mm), the minimum rotating speed of the metering disc is calculated to be 593.5 rad/min, corresponding to a minimum sowing speed of 4.08 km/h. When the sowing speed approaches the minimum value, the centrifugal force acting on the seeds is small, resulting in a low seed-filling rate and insufficient seed clearing, which in turn leads to poor number of seeds normally sown (quality of feed index>90%, miss index <5% and multiples index <5%) of the metering device. To achieve high-performance high-speed metering, greater centrifugal force is required for both seed filling and seed clearing. Therefore, the

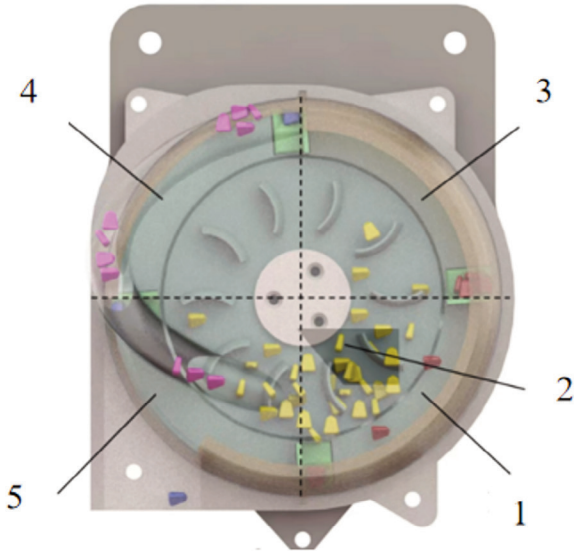

Figure 2. Schematic diagram of the working process of the metering device. 1. seed-filling zone; 2. chamber; 3. seed-carrying zone; 4. seed-clearing zone; 5. seed-dropping zone.

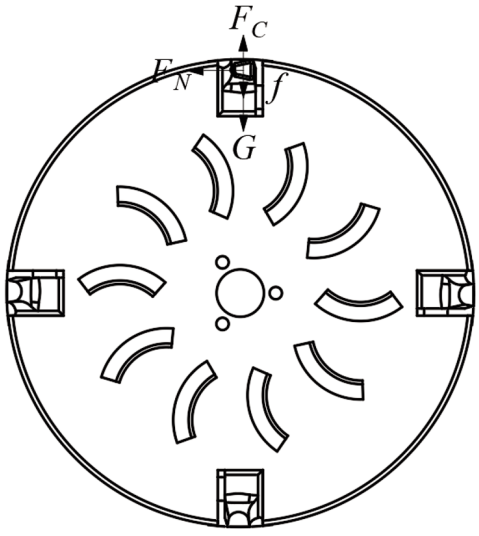

Figure 3. Seed force analysis at the topmost point of the metering disc.

sowing speed should be greater than 4.08 km/h. To realize high-speed precision seeding, the forward speed of the seeder should exceed 8 km/h, and accordingly, the rotating speed of the metering disc should be greater than 1163 rad/min.

Design of the seed-protecting plate

The seed-protecting plate assists the seed cells in completing key steps such as seed filling, seed carrying, and seed clearing during the operation of the metering device. Its functions span the entire working process of the metering device, and thus the seed-protecting plate has a significant impact on the overall performance of the device. During operation, the direction of the gravitational force on the seeds changes relative to the radial direction. The force analysis of the seeds at the bottom of the chamber satisfies Eq. (4).

$$\begin{cases} F_N = (F_C + G)\cos\alpha \\ f = \mu F_N \\ F_T = (F_C + G)\sin\alpha - f \end{cases} \quad \text{(Eq. 4)}$$

where: F_N is the supporting force acting on the maize seed (N); μ is the static friction coefficient; α is the inclination angle of the constraint surface (°); F_T is the resultant force in the seed-filling direction (N).

During the seed-filling process, for seeds to successfully fill into the seed cells, F_T should be greater than zero. As α increases, both F_N and the friction force (f) decrease, while F_T increases. Under critical conditions, the inclination angle α of the seed-protecting plate satisfies Eq. (5).

$$\alpha = arctan\ \mu \quad \text{(Eq. 5)}$$

The static friction coefficient between maize seeds and POM is 0.46. According to the equation, the inclination angle α is calculated to be 24.7°. To ensure that seeds can successfully fill to the bottom of the seed cells, the inclination angle of the seed-protecting plate should be greater than 24.7°. A larger inclination angle leads to a greater resultant force in the filling direction, which is more favorable for rapid seed filling. Therefore, the inclination angle is finally set to 30°.

During the seed-filling process, the seed-protecting plate cooperates with the seed cells, and its structural parameters mainly include the front-end width W_1 of the seed-protecting plate in the seed-filling zone, the front-end width W_2 of the seed-protecting plate in the seed-clearing zone, and the width W_3 of the seed-protecting plate in the seed-delivering zone. These parameters collectively ensure that the seed-protecting plate can meet seed requirements at each stage. The dimensions of each part of the seed-protecting plate should satisfy Eq. (6).

$$\begin{cases} \frac{3}{2}l_0 < W_1 < \frac{5}{2}w_0 \\ \frac{1}{2}t_0 < W_2 < \frac{3}{2}t_0 \\ h_1 < W_3 < \frac{1}{2}t_0 + h_2 \end{cases} \quad \text{(Eq. 6)}$$

where: l_0 is the average length of the seeds (mm); w_0 is the average width of the seeds (mm); t_0 is the average thickness of the seeds (mm); h_1 is the distance between the bottom of the metering disc and the bottom of the seed cell (11 mm); h_2 is the distance between the bottom of the metering disc and the bottom of the seed cell (13.5 mm). Comprehensively considering these factors, the front-end width W_1 of the seed-protecting plate in the seed-filling zone, the front-end width W_2 of the seed-protecting plate in the seed-clearing zone, the width W_3 of the seed-protecting plate in the seed-dropping zone, and the front-end inclination angle α of the seed-protecting plate are set to 15.5 mm, 2 mm, 12.5 mm, and 30°, respectively. The structure of the seed-protecting plate is shown in Figure 4.

Design of the seed cell

The seed cell is in direct contact with the seeds, and therefore its structural shape and parameters have a significant impact on the operational performance of the metering device. Studies have shown that maize seeds achieve maximum contact area and relatively stable posture when lying flat within the seed cell, which is beneficial for effective seed filling. Thus, the higher the proportion of seeds lying flat during filling, the better the metering performance (Li *et al*., 2025). To improve the performance of the seed cell, its design was based on the seed dimensions and contours (Liu *et al*., 2015). The structural parameters of the seed cell include the aperture length (L), aperture width (W), aperture depth (H), right corner radius (R), rear wall inclination angle (γ), ear height (E), seed-protecting plate height (h), and front inclination angle of the aperture, which is consistent with the front inclination angle of the seed-protecting plate at 30°, effectively preventing seeds from becoming stuck inside the seed cell, as shown in Figure 5. To ensure a high seed-filling success rate, the dimensions of the seed cell should be larger than those of the maize seeds, allowing multiple seeds to enter the cells during the filling process. Through the special design of the cell, the number of seeds filling into the cells can be effectively controlled to prevent overcrowding.

After the seed cell is filled with seeds, seeds can become easily stuck inside the cell, leading to missed seeding. When a maize seed gets stuck in the seed cell, the stress on one end of the seed can be analyzed. The primary force causing the seed to leave the seed cell is the centrifugal force, while gravity is neglected in this analysis. When the centrifugal force (F_c) equals the friction force (f)

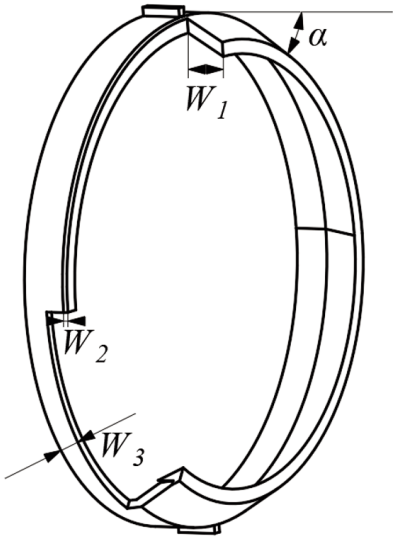

Figure 4. Structure diagram of seed-protecting plate.

between the seed and the seed cell, the resultant force F_T becomes zero, causing the seed to remain stuck inside the seed cell and resulting in missed seeding. The opening of the seed cell is gradually expanded forward at an acute angle (θ), which can effectively prevent seeds from getting stuck. A force analysis of one end of the maize seed is illustrated in Figure 6 and satisfies Eq. (7).

$$\begin{cases} F_2 = F_N \cos\theta \\ f_1 = \mu F_N \sin\theta \\ F_T = F_c + F_2 - f_1 \end{cases} \quad \text{(Eq. 7)}$$

where: μ is the static friction coefficient; F_N is the supporting force acting on the maize seed (N); f_1 is the radial component of the friction force f; F_2 is the radial component of the supporting force F_N (N); F_T is the resultant force in the seed-filling direction (N).

When the supporting force (F_N) is constant, a decrease in the acute angle (θ) leads to a reduction in f_1, an increase in F_2, and thus an increase in the resultant force (F_T). When the acute angle (θ) decreases to a certain value, the resultant force becomes greater than zero, allowing the maize seed to exit the seed cell. From the analysis of the interaction forces between the seed and the inner wall of the cell, it can be concluded that whether the seed becomes stuck in the cell depends only on the acute angle (θ) and the length of the cell, with no direct relationship to other parameters. To determine the optimal acute angle of the cell opening, a set of preliminary experiments was conducted using seed cells with different acute angles and lengths. The results indicated that the optimal acute angle (θ) for the seed cell opening is 80°.

The EDEM software was used to analyze the seed postures during the seed-filling process of the metering device, as shown in Figure 7. The forces acting on the seeds follow Eq. (8).

$$\begin{cases} F_{N1} = \dfrac{F_c \cos\varphi_1}{\cos\varphi_2} \\ M_1 = (F_{f1}\cos\varphi_2 - F_{N1}\sin\varphi_2)D_1 \end{cases} \quad \text{(Eq. 8)}$$

where: F_c is the centrifugal force (N); F_{N1} is the supporting force acting on the seed from the barrier surface (N); F_{f1} is the component of the friction force (N); D_1 is the distance from the seed's center of mass to the contact point (mm); φ_1 is the angle between the straight line connecting the center of mass and the contact point and the direction of the centrifugal force (°); φ_2 is the angle between the straight line connecting the center of mass and the contact point and the direction of the supporting force (°); M_1 is the rotational torque (N·m). When the rotational torque is nonzero, seeds will rotate, and under the effect of the rotational torque, the final posture of the seeds becomes either upright or semi-recumbent. Therefore, under different metering speeds, the seed postures during seed filling are predominantly upright or semi-recumbent. In a few cases, multiple seeds may simultaneously enter the cell and stack together, resulting in other filling postures. Simulation results revealed that when the cell length is less than 9.5 mm, the number of misses under different forward speeds is relatively high. The main reason for missed seeding is that when the cell length is less than 9.5 mm, the seeds do not enter the cell in an upright or semi-recumbent posture, leading to seeds getting stuck and failing to exit. The force analysis of the seeds under such conditions is shown in Figure 8 (a) and satisfies Eq. (9).

$$\begin{cases} F_{N1} = F_c \cos\beta \\ F_{N3} = F_{N4}\sin\sigma - F_{f4}\cos\sigma \\ F_T = F_c\sin\beta - F_{f1} - F_{f3} - F_{N4}\cos\sigma - F_{f4}\sin\sigma \end{cases} \quad \text{(Eq. 9)}$$

where: F_{N3} is the supporting force from the left wall of the cell (N); F_{N4} is the supporting force from the right corner (N); F_{f1}, F_{f3}, and F_{f4} is the friction force components acting on the seed in various directions (N); β is the front inclination angle of the cell (°); σ is the angle between the friction force and the horizontal axis (°).

When multiple seeds are stuck at the cell opening, and there is no relative movement among them, they can be considered as an integrated body. At this point, the force analysis of the maize seeds is shown in Figure 8b and still follows Eq. (9). When the supporting forces and friction forces on the seeds are large, the resultant force becomes zero, causing the seeds to remain stuck and preventing them from successfully reaching the bottom of the cell. These stuck seeds are eventually cleared during the seed-clearing process, leading to a higher number of misses. As the cell length increases, when the cell length reaches 9.5 mm or more, the force analysis of the seeds is shown in Figure 8c, satisfying Eq. (10). In this case, the centrifugal force component in the seed-filling direction is greater than the friction force, and the resultant force becomes positive. Thus, the number of misses decreases significantly. However, as the cell length continues to increase, the number of multiples also increases. According to the simulation results, under different forward speeds, the number of seeds normally sown is similar, and the cell length is 9.5 mm.

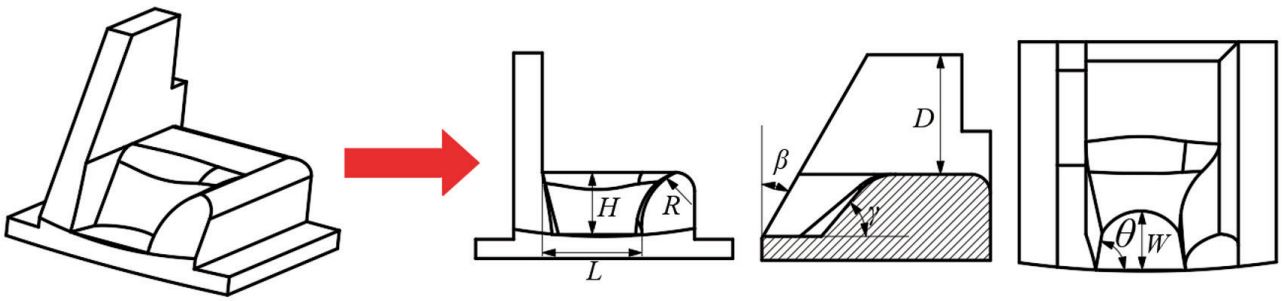

Figure 5. Structural diagram of the seed cell.

$$\begin{cases} F_{N1} = F_c \cos\beta \\ F_T = F_c \sin\beta - F_{f1} \end{cases} \quad \text{(Eq. 10)}$$

The length of the seed cell was set to 9.5 mm, and different seed cells with varying widths were designed at 1 mm intervals. Simulation tests were conducted under different forward speeds to determine the optimal width of the seed cell. When the cell width is relatively small, the seed width becomes greater than the cell width, causing the seed to enter the cell in a sideways posture, leading to the seed becoming stuck inside the cell. The force analysis when the seed is follows Eq. (11).

$$\begin{cases} F_{N1} = F_c \cos\beta + F_{N5} \cos\sigma - F_{f5} \sin\sigma \\ F_T = F_c \sin\beta - F_{f1} - F_{N5} \sin\sigma - F_{f5} \cos\sigma \end{cases} \quad \text{(Eq. 11)}$$

where: F_{N5} is the supporting force from the rear wall of the seed cell (N); F_{f1} and F_{f5} is the components of the friction forces acting on the seed in various directions (N).

When the seed encounters the rear wall, a large supporting

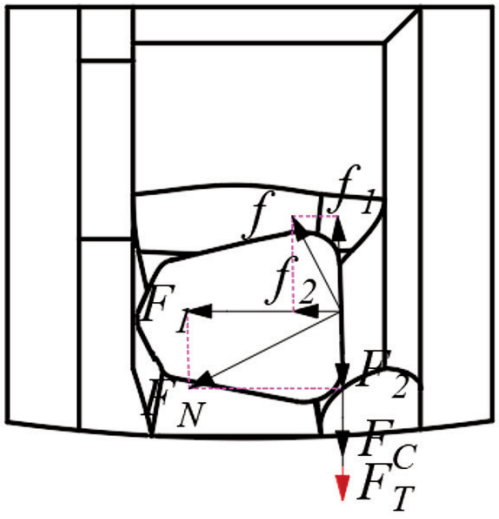

Figure 6. Force analysis at one end of the seed inside the seed cell.

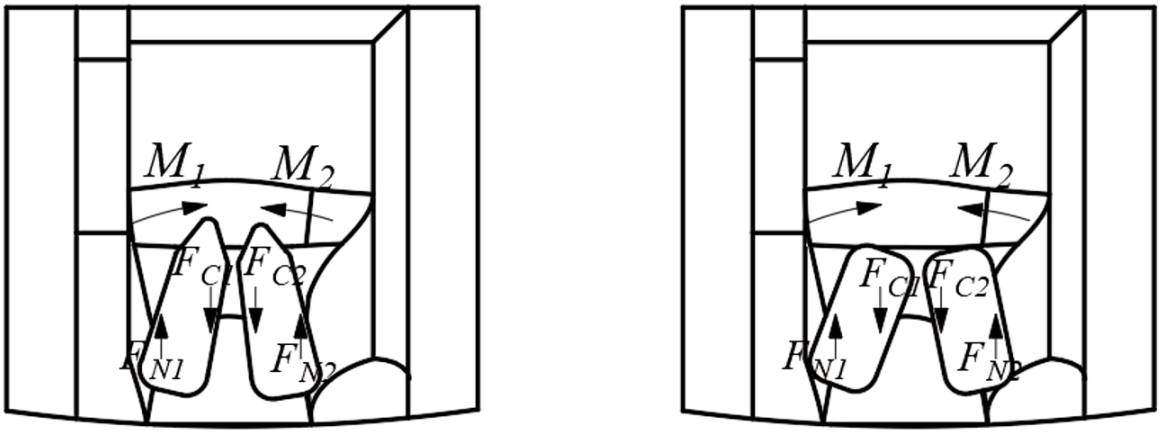

Figure 7. Posture changes of seeds during the seed-filling process.

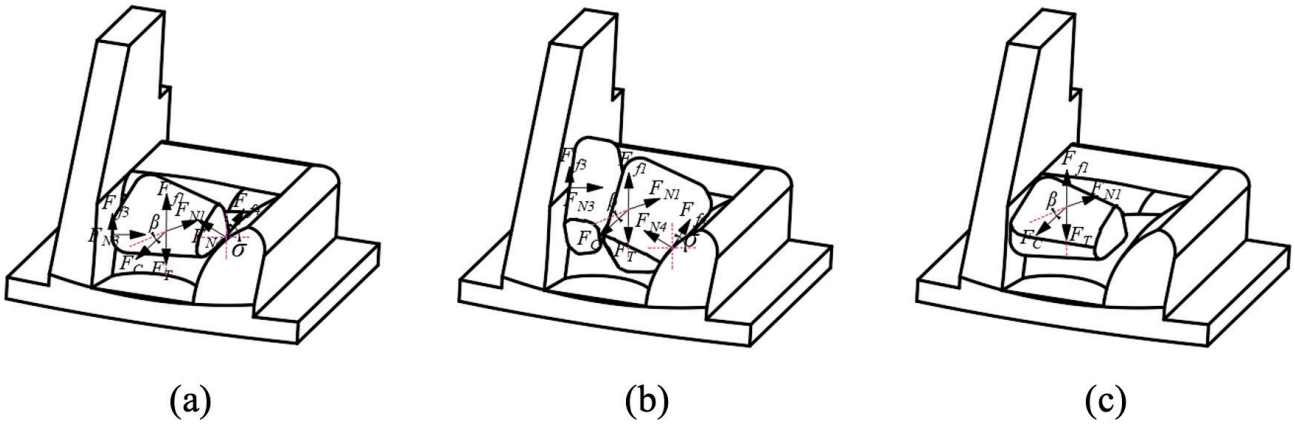

Figure 8. Force analysis of seeds under different cell lengths. **a**) Cell length is less than 9.5 mm. (**b**) Multiple seeds are stuck at the cell opening. **c**) Cell length reaches 9.5 mm or more.

force and friction force are generated, causing the resultant force in the seed-filling direction to become zero. As a result, the seed becomes stuck and cannot be filled to the bottom of the cell. During the seed-clearing process, these stuck seeds are entirely cleared out, leading to a high number of misses. As the cell width increases, when the bottom width of the cell approaches twice the seed thickness, multiple seeds may be discharged simultaneously, resulting in a gradual increase in the number of multiples. Different cell widths were designed at 0.5 mm intervals, and it was ultimately determined that when the cell width is 6.5 mm, the metering device achieves seeds normally sown.

The depth of the seed cell influences the effective height of the seed-protecting plate in the seed-clearing zone, which can lead to excessive or insufficient seed clearing and consequently affect normally sown. The dimensions of the seed-protecting plate in the seed-clearing zone were determined based on the average dimensions of the seeds. To ensure that the seeds can fully enter the seed cell, the final cell depth was set to 6.5 mm.

When the seed is located at the right corner of the cell, the angle between the supporting force and the vertical axis increases the resultant force toward the left, thus accelerating the seed's movement toward the center of the cell. Simultaneously, due to the same angular effect, the resultant force in the seed-filling direction also increases, accelerating the filling of the seed toward the bottom of the cell. When the radius of the right corner is relatively small, seeds cannot smoothly enter the cell, leading to insufficient seed filling and an increase in the number of misses. As the radius of the right corner increases, seeds can smoothly fill into the cell, thereby reducing the number of misses. However, the number of multiples also increases accordingly. Different seed cells with varying right corner radii were designed at 1 mm intervals and were verified through simulation. The force analysis of the seeds under this condition satisfies Eq. (12). Based on experimental verification, it was finally determined that the seeds normally sown is achieved when the right corner radius of the cell is set to 7 mm.

$$\begin{cases} F_{N1} = F_c \cos\beta \\ F_{T1} = F_{N4} \sin\sigma - F_{f4} \cos\sigma \\ F_T = F_c \sin\beta - F_{f1} - F_{N4} \cos\sigma - F_{f4} \sin\sigma \end{cases} \quad \text{(Eq. 12)}$$

Based on the above analysis, the optimal structural parameters of the seed cell were obtained. The rear wall inclination angle of the seed cell also has a significant effect on seed-filling performance. Seed cells with different rear wall inclination angles, designed at 5° intervals, were subjected to simulation tests for verification. When the rear wall inclination angle is relatively small, the inlet size of the cell is larger. Therefore, during seed filling, seeds can easily enter the cell, resulting in a lower number of misses. However, the occurrence of multiple seeds entering simultaneously increases, leading to a higher number of multiples. As the rear wall inclination angle increases, the inlet size decreases, making it more difficult for seeds to enter during filling, and increasing the likelihood of seeds getting stuck, which raises the number of misses. When the rear wall inclination angle (γ) is set to 50°, the metering device demonstrates normally sown.

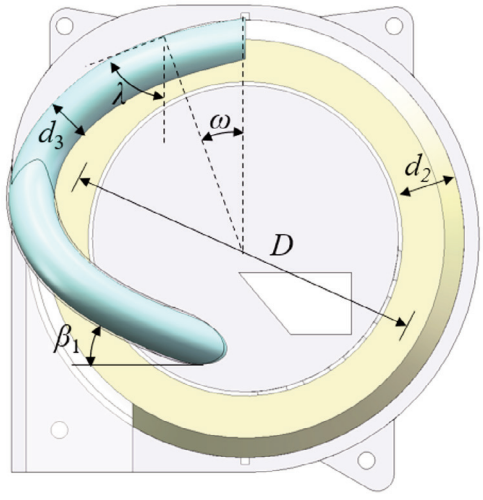

Figure 9. Structural diagram of the front housing.

The height of the cell ear affects the seed-capturing ability of the seed cell. When the cell ear height is small, its ability to capture seeds is weak, resulting in fewer seeds entering the seed cell and an increased number of misses. As the cell ear height increases, the seed-capturing ability of the seed cell improves, and the number of misses gradually decreases. However, excessive seed capture can also reduce seed-clearing efficiency, leading to an increase in the number of multiples. According to the simulation results, when the cell ear height is set to 12.5 mm, the seed-capturing performance is optimal.

Design of the front housing

The front housing mainly consists of the seed-filling chamber, the annular chamber, and the return pipe, with the seed-filling chamber and the annular chamber separated by a partition plate. The inner diameter of the annular pipe is denoted as d_2, the inner diameter of the return pipe as d_3, the diameter of the annular pipe as D, the radius of the return duct as R_1, the return angle as β_1, the seed-clearing angle as ω, and the inclination angle of the seed-clearing opening as λ, as shown in Figure 9. The average length of maize seeds generally ranges from 9 mm to 14 mm. When designing the return pipe, it is necessary to ensure that maize seeds can pass through the pipe one by one without becoming stuck. Therefore, the inner diameter (d_3) of the return duct should satisfy the following Eq. (13):

$$d_{max} + J < 2R_1 < 2d_{max} + J \quad \text{(Eq. 13)}$$

where: d_{max} is the maximum average length of the maize seeds (mm); R_1 is the radius of the return pipe (mm); J is the wall thickness of the return pipe (mm).

To ensure that maize seeds can smoothly pass through the return pipe and re-enter the metering device, the inner diameter (d_3) of the return pipe was finally determined to be 22 mm. Given that the diameter of the metering disc is 200 mm and the side width of the seed cell is 23 mm, to achieve the isolation effect and allow seeds to pass through the aperture structure into the pipe, thereby completing the transition from the waiting zone to the seed-filling zone, the seed cells must be fully placed within the annular pipe structure. Therefore, the inner diameter of the annular pipe must satisfy the following conditions:

$$d_2 > W_1 \quad \text{(Eq. 14)}$$

where: d_2 is the inner diameter of the annular pipe (mm); W_1 is the side width of the seed cell (mm).

The seed-clearing opening is one of the critical factors affecting the return efficiency. The inlet of the return pipe was designed

based on the position of the seed-clearing opening. An accurate design of the seed-clearing opening position facilitates the discharge of excess seeds and promotes precise single-seed filling. When the seed detaches from the seed cell, the rotating angle of the metering disc can be calculated according to its motion Eq. 15:

$$\begin{cases} L_1 = \frac{1}{2} a_1 t_1^2 \\ v_1 t = \omega r \\ a = \frac{v_1^2}{r} \end{cases} \quad \text{(Eq. 15)}$$

where: L_1 is the distance traveled by the seed after detaching from the seed cell (mm); a_1 is the centripetal acceleration of the seed (m/s²); t is the time during which the seed detaches from the seed cell (s); v_1 is the linear velocity of the metering disc (m/s); r is the radius of the metering disc (mm).

Since the centrifugal force acting on the seed during the high-speed operation of the metering device is much greater than its gravitational force, the effect of gravity on the seed can be neglected. By rearranging the above equation, the following equation is obtained:

$$\omega = \sqrt{\frac{2L_1}{r}} \quad \text{(Eq. 16)}$$

From Eq. (16), it can be concluded that the rotating angle (δ) of the metering disc during the seed's detachment process depends only on the distance (L_1) traveled by the seed after detaching from the seed cell and the radius (r) of the metering disc, and is independent of the rotating speed of the disc. Therefore, the position of the seed-clearing point does not change with the forward speed. Based on calculations, the angle (ω) is approximately 30°, and thus the seed-clearing opening of the return pipe was designed tangentially to the cleaning point, with an included angle of 60° relative to the metering device.

Since the distance from the seed box to the lowest point of the metering device is 65 mm, the maximum seed accumulation height after seeds enter the metering device is also 65 mm. Given that the friction angle of maize seeds is 28°, and the return angle β_1 of the return pipe is set to 28°, the center of the return pipe was positioned at 65 mm from the lowest point of the metering device, maintaining the same height as the seed box. This design ensures that when seeds re-enter the metering device from the return pipe for re-filling, they will not become stuck at the inlet of the pipe.

In summary, the diameter (D) of the annular pipe was determined to be 175 mm, the inner diameter (d_2) of the annular pipe was set to 30 mm, the inner diameter (d_3) of the return pipe was set to 22 mm, and the return angle (β_1) was set to 28°. To prevent excessive seed accumulation near the seed cells, which may result in multiple seeds being filled into a single cell and cause reseeding errors, a pipe structure was incorporated within the internal chamber of the seed metering device. Apertures were arranged in the seed filling zone of the pipe to control entry. After seeds enter the metering device from the seed box, they fall into the bottom of the metering disc under the influence of gravity and accumulate in the waiting zone. Driven by the seed-disturbing teeth on the metering disc, the seeds begin to move within the chamber. A portion of the seeds in the waiting zone passes through the apertures into the pipe structure and are subsequently loaded into the seed cells, thereby completing the seed filling process. To accommodate the shape of maize seeds, preliminary research determined that the aperture should be circular. To ensure that maize seeds can pass smoothly through the apertures and enter the seed filling zone, the diameter of the circular apertures should be greater than the average seed length. However, to prevent an excessive number of seeds from passing through and accumulating near the seed cells, the diameter should not exceed twice the average seed length. The recommended range for the aperture diameter is defined as follows:

$$l_0 < l_c < 2l_0 \quad \text{(Eq. 17)}$$

where: l_0 is the average length of the seeds (mm); l_c is the diameter of the circular aperture (mm).

Based on statistical calculations, the diameter of the circular apertures was determined to be in the range of 13-15 mm.

Design of seed-disturbing teeth

Single-seed pickup is a critical factor in achieving mechanized maize seeding. Due to the relatively high surface roughness of maize seeds, particle accumulation is prone to occur. To enhance the flow-ability of maize seeds and enable them to pass smoothly through the apertures into the seed cells for seed filling -thus avoiding seed blockage caused by accumulation- seed-disturbing teeth were designed on the metering disc to promote the movement of seeds within the chamber. The structural parameters of the seed-disturbing teeth include the involute profile and the protrusion height of the teeth. After extracting multiple profile curves of maize seeds, a parabolic curve was fitted. The fitted parabolic equation can be obtained, and the vertex of the parabola passes through the origin, satisfying Eq. (18).

$$\begin{cases} x^2 = 2py \\ y = kx + b \end{cases} \quad \text{(Eq. 18)}$$

where: x is the horizontal coordinate of the involute (mm); y is the vertical coordinate of the involute (mm); p is the distance from the parabola's focus to its directrix (mm); b is the intercept (mm); k is the slope.

When k = tan 54°, the parabolic equation of the curve is derived as:

$$x^2 = 2.97y \quad \text{(Eq. 19)}$$

Based on the similarity between the fitted involute profile and the profile of maize seeds, the structural parameters of the seed-disturbing teeth were designed according to the actual seed dimensions to satisfy the following Eq. (20):

$$\begin{cases} l_0 < l < l_{ab} < l_{cd} \\ w_0 \le h \\ r_2 - r_1 \le \frac{h}{2} \\ x = x_0 + s\cos\varphi \\ y = y_0 + s\sin\varphi \end{cases} \quad \text{(Eq. 20)}$$

where: l is the length of the seed-disturbing teeth (mm); l_{ab} is the distance between two disturbing teeth at points a and b (mm); l_{cd} is the distance between two seed-disturbing teeth at points c and d

(mm); w_0 is the average width of the seeds (mm); h is the width of the seed-disturbing teeth (mm); r_2 is the outer radius of the seed-disturbing teeth (mm); r_1 is the inner radius of the seed-disturbing teeth (mm); s is the base circle radius (mm); φ is the rotating angle of the radius s around the center of the circle (°).

Based on the average particle size of maize seeds and the external profile equation of the maize seed, it was found that, when designing the left and right profiles of the seed-disturbing teeth, the parabola within the range of $l \in$ (−16 mm, 16 mm) approximates a circular structure. To meet both the machining process requirements and the parabola opening size, the left and right profiles of the seed-disturbing teeth were designed as concentric circular arcs, with radii of 20 mm and 28 mm, respectively. This design provides a larger accommodating space compared to the original parabola. In addition, the upper and lower profiles of the seed-disturbing teeth were formed by circular arcs passing through the center of the metering disc, with radii of 32 mm and 69 mm, respectively. The intersections of these four in volute curves define the external profile of the seed-disturbing teeth. Accordingly, the distance between two seed-disturbing teeth at points a and b was designed to be 20 mm, and the distance between points c and d was set to 42 mm. The height of the seed-disturbing teeth on the metering disc was designed to be 10 mm.

Design of the seed box

The seed box is one of the core components of the maize metering device. The structural dimensions and shape of the seed box directly affect the flow-ability of the seeds inside. If the design of the structural dimensions and shape is unreasonable, it may lead to seed compression, breakage, or bridging within the seed box, resulting in uneven seeding or even missed seeding. To ensure that seeds can move smoothly within the seed box without being damaged, the shape and structural dimensions of the seed box were designed based on the physical characteristics and dimensional parameters of maize seeds. The volume of the seed box should be set according to the row spacing and inter-row spacing of the metering device to ensure that it can store enough seeds without becoming excessively heavy. The volume of the seed box is calculated by the following Eq. (21):

$$V = \frac{S_V \times M}{\rho v} \quad \text{(Eq. 21)}$$

where: V is the volume of the seed box (m³); S_V is the seeding area supported by one filling of the seed box (mu); M is the seeding rate per unit area of the metering device (g/mu); ρ_v is the bulk density of maize seeds (g/L). To prevent mutual interference between adjacent components, the maximum width of the seed box was set to 80 mm, and its volume was determined to be 200 mL. To ensure that seeds can be smoothly delivered into the metering device, the lower outlet of the seed box must align with the seed inlet of the metering device. Considering that all seeds must enter the metering device completely during seeding, the lower part of the seed box was designed in a conical shape. Given that the repose angle of maize seeds is 26°, the cone angle of the lower section was set to 40°. This design improves the seed box volume while ensuring that the seed filling rate is not adversely affected.

The height of the seed box is closely related to the seed pile inside the metering device. If the seed box is set too high, an excessive number of seeds will enter the metering device, leading to overfilling and an increased occurrence of reseeding. Conversely, if the seed box is set too low, too few seeds will enter the metering device, resulting in under-filling and a higher number of misses. Experiments were conducted by setting the seed box at different heights. Ultimately, the height of the seed box was determined to be 65 mm above the lowest point of the metering device. As seeds continuously enter from the seed box into the metering device, they are disturbed by the seed-disturbing teeth, promoting movement within the chamber. Given that the lower profile line of the seed-disturbing teeth forms a circular arc with a radius of 69 mm centered on the metering disc, setting the seed box at a height of 65 mm above the lowest point effectively controls the seed flow rate and prevents seed accumulation at the apertures, which could otherwise cause seed blockage.

Bench test

Test materials and setup

The metering device used in the test was the independently developed layered centrifugal mechanical high-speed precision maize metering device. The test bench was self-designed and constructed, as shown in Figure 10. The custom-designed bench test system consists primarily of an STM32 micro-controller as the control unit. A Pufeide 86HSE12N closed-loop stepper motor, paired with an HBS86H driver, was employed as the actuation module for the seed metering device. The motor speed was controlled via STM32's PWM-based timer module. A human-machine interface program was developed to manage communication between a touchscreen serial display and the controller, enabling real-time display and adjustment of operational parameters. High-speed imaging (Qianyanlang M230) was used in conjunction with a data acquisition system to conduct performance optimization experiments for the seed metering device.

The seeds used in the test were ungraded hybrid seeds of the variety Zhengdan 958, consistent with actual seeding conditions. Based on their outer contours, they are classified into three types: large flat, small flat, and nearly spherical. One thousand seeds were selected from the test samples for length, width, and thickness measurement (Ding *et al*., 2018), and the results are shown in Table 1. During the test, the plant spacing was set to 180 mm. According to the standard ISO 7256/1 (Sowing equipment; Test methods), the quality of feed index (A), the multiples index (D), and the miss index (M) were selected as the evaluation indicators.

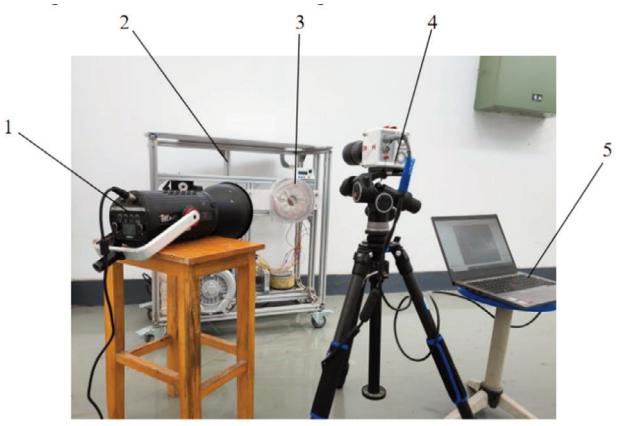

Figure 10. Test equipment. 1. fill light; 2. test bench; 3. seed metering device; 4. high-speed camera; 5. PC.

Test design

To obtain an optimal combination of operating parameters for the metering device, a three-factor, three-level central composite orthogonal experiment was designed based on theoretical analysis and preliminary experimental exploration (Liao *et al*., 2022; Ma *et al*., 2024). The rotating speed of the metering disc, the number of apertures, and the diameter of the aperture were selected as the experimental factors. The factor levels are shown in Table 2. Continuous 251 seeds were collected from each experimental group, and each group was repeated three times, and the average value was analyzed. During the test, the initial number of seeds in the seed box was 50 % of total volume of the hopper. The operation stop time is 12.5 % of the total volume of the hopper.

Results

Analysis of bench test results

The experimental arrangements and results are shown in Table 3.

Regression modeling and significance analysis

Design-Expert 8.0.6 (Stat-Ease, Inc., Minneapolis, USA) was used to analyze and fit the experimental data. Regression fitting was performed on the experimental results, and the regression model was established, as shown in Eq. (22). The significance test results are presented in Table 4.

$$A = 92.02+0.26X_1+0.12X_2-0.68X_3+1.04X_1X_2+0.88X_2X_3-1.84X_1^2-5.26X_2^2-2.70X_3^2$$
$$D = 5.6-2.35X_1+0.83X_2+0.47X_3+1.29X_1X_3-0.64X_2X_3+0.53X_1^2+2.70X_2^2+0.41X_3^2$$
$$M = 2.37+1.91X_1-0.92X_2-0.02X_3-1.23X_1X_2+1.45X_1^2+2.73X_2^2+2.37X_3^2$$

(Eq. 22)

According to Table 4, the model for the quality of feed index exhibits a highly significant fit ($p<0.01$, When the p-value is between 0.01 and 0.05, it indicates a significant effect. When the p-value is less than 0.01, it indicates a highly significant effect.).

Table 1. Three-dimensional dimensions of maize seeds.

Type	3D dimensions	Measured value
Large flat shape	Length (mm)	8.2-14
	Width (mm)	5.5-11.3
	Thickness (mm)	3.6-7.5
Small flat shape	Length (mm)	7.2-12.6
	Width (mm)	5.1-10.1
	Thickness (mm)	3.3-7.0
Quasi-round	Length (mm)	8.5-12.1
	Width (mm)	7.0-10.6
	Thickness (mm)	5.0-9.9

Table 2. Coding of test factors.

Code	Rotating speed X_1 (rad/min)	Number of apertures X_2	Aperture diameter X_3 (mm)
-1	1507.2	413	
0	1695.6	514	
1	1884.0	615	

Table 3. Test design and results.

Order	X_1 (rad/min)	X_2	X_3 (mm)	A (%)	D (%)	M (%))
1	1507.2	4	14	85.33	10.40	4.27
2	1884.0	4	14	83.65	5.60	10.76
3	1507.2	6	14	84.10	11.98	4.80
4	1884.0	6	14	86.59	7.37	6.38
5	1507.2	5	13	86.69	9.94	4.22
6	1884.0	5	13	88.63	2.69	8.68
7	1507.2	5	15	87.62	7.83	4.55
8	1884.0	5	15	86.97	5.72	7.32
9	1695.6	4	13	86.31	6.55	8.14
10	1695.6	6	13	84.16	9.46	6.38
11	1695.6	4	15	82.19	9.24	8.57
12	1695.6	6	15	83.56	9.61	6.83
13	1695.6	5	14	91.54	5.67	2.79
14	1695.6	5	14	91.33	5.76	2.91
15	1695.6	5	14	92.65	5.36	1.99
16	1695.6	5	14	91.97	5.85	2.19
17	1695.6	5	14	92.63	5.38	1.99

However, the *p*-values of the linear term for rotating speed (X_1), the number of apertures (X_2), and the interaction term between rotating speed and mesh cell diameter (X_1X_3) are all greater than 0.1, indicating that their effects on the quality of feed index are not significant. All other terms are significant, suggesting that the selected experimental factors exhibit quadratic relationships with the response indicator. Based on the coefficient analysis, the order of influence on the quality of feed index can be ranked as follows: aperture diameter, rotating speed, and number of apertures. This result indicates that the working speed does not significantly affect the quality of feed index, demonstrating that the operating principle and structure of the metering device are well-suited for high-speed operations. The model for the multiples index exhibits a highly significant fit ($p<0.01$). However, the *p*-value of the interaction term X_1X_2 is greater than 0.1, indicating that its effect on the multiples index is not significant. All other terms are significant, suggesting

Table 4. ANOVA for the regression model.

Source of variation	A		D		M	
	F	*p*	*F*	*p*	*F*	*p*
Model	34.56	<0.0001**	110.25	<0.0001**	65.52	<0.0001**
X_1	0.89	0.3735	466.63	<0.0001**	151.88	<0.0001**
X_2	0.18	0.6864	58.22	0.0001**	35.05	0.0006**
X_3	6.08	0.0430*	18.72	0.0034**	0.01	0.9072
X_1X_2	7.12	0.0320*	0.10	0.7661	31.28	0.0008**
X_1X_3	2.75	0.1413	69.98	<0.0001**	3.71	0.0956
X_2X_3	5.08	0.0589	17.09	0.0044**	0.0005	0.9825
X_1^2	23.41	0.0019**	12.61	0.0093**	45.66	0.0003**
X_2^2	191.22	<0.0001**	325.65	<0.0001**	163.24	<0.0001**
X_3^2	50.47	0.0002**	7.47	0.0292*	123.06	<0.0001**
Lack of fit	2.52	0.1966	3.09	0.1518	0.88	0.4982

*$p<0.05$; **$p<0.01$.

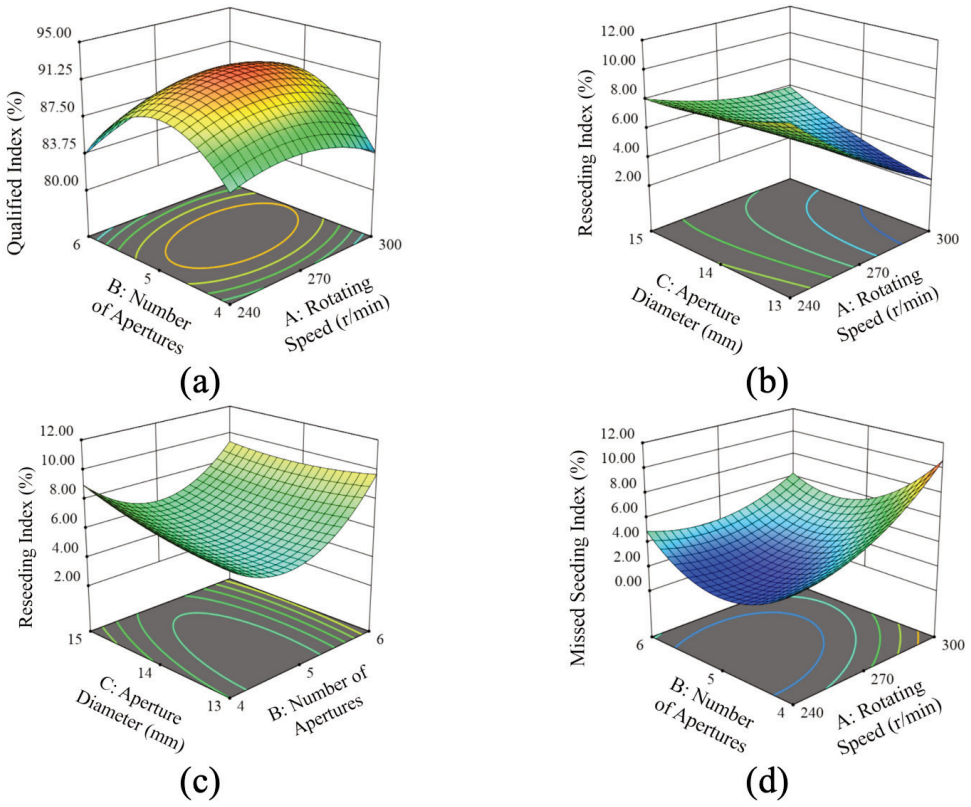

Figure 11. Effects of experimental factors on each performance indicator. **a)** Quality of feed index: interaction diagram of number of apertures and rotating speed. **b)** Multiples index: interaction diagram of aperture diameter and rotating speed. **c)** Multiples index: interaction diagram of aperture diameter and number of apertures. **d)** Miss index: interaction diagram of number of apertures and rotating speed.

that the selected experimental factors exhibit quadratic relationships with the response indicator. The order of influence on the multiples index can be ranked as follows: rotating speed, number of apertures, and aperture diameter. The model for the miss index exhibits a highly significant fit ($p<0.01$). However, the p-values of the linear term for aperture diameter (X_3), the quadratic interaction terms X_1X_3 (between rotating speed and aperture diameter) and X_2X_3 (between number of apertures and aperture diameter) are all greater than 0.1, indicating that their effects on the miss index are not significant. All other terms are significant, suggesting that the selected experimental factors exhibit quadratic relationships with the response. The order of influence on the miss index can be ranked as follows: rotating speed, number of apertures, and aperture diameter.

Response surface analysis of significant interaction terms on performance indicators

To analyze the relationships between the factors and the performance indicators, response surface diagrams of the experimental results were generated using Design-Expert software, as shown in Figure 11. Figure 11a illustrates the effects on the quality of feed index: the quality of feed index initially increases and then decreases with the increase in rotating speed, reaching a maximum value within the range of 1632.8-1758.4 rad/min. The quality of feed index first increases and then decreases with the increase in the number of apertures, reaching a maximum at approximately 4.5~5.5 apertures. Figure 11b,c shows the effects on the multiples index. The multiples index decreases first and then increases with the increase in the number of apertures, reaching a minimum at approximately 4.5~5.5 apertures. The multiples index decreases with the increase in rotating speed, indicating that a higher rotating speed improves the seed-cleaning performance, thus reducing the multiples index. The multiples index increases with the increase in aperture diameter, as larger apertures allow more seeds to enter the seed cells, making seed clearing more difficult and thereby increasing the multiples index, with a minimum observed around 13~14 mm. Figure 11d illustrates the effects on the miss index. The miss index decreases first and then increases with the increase in the number of apertures, reaching a minimum at approximately 4.5~5.5 apertures. The miss index increases with the increase in rotating speed, as higher rotating speeds improve seed clearing but can also lead to excessive seed clearing.

Parameter optimization and validation experiment

The optimization was conducted by selecting the condition where the quality of feed index was maximized while the multiples index and the miss index were minimized, combined with appropriate factor constraints.

$$\begin{cases} \max M(X_1, X_2, X_3) \\ \min A(X_1, X_2, X_3) \\ \min D(X_1, X_2, X_3) \\ s.t. \begin{cases} 240 \le X_1 \le 300 \ rad/min \\ 4 \le X_2 \le 6 \\ 13 \le X_3 \le 15 \ \text{mm} \end{cases} \end{cases} \quad \text{(Eq. 23)}$$

The normally sown was achieved when the rotating speed was 1729.01 rad/min, the number of apertures was 5, and the aperture diameter was 14 mm. Under these conditions, the quality of feed index reached 92.07%. To verify the reliability of existing results, a validation experiment was conducted under the same conditions to verify its authenticity and accuracy, yielding a quality of feed index of 92.10%. This result demonstrates that optimization is reliable.

Conclusions

i) Leveraging the characteristics of high-speed operations, a layered centrifugal mechanical high-speed precision maize metering device was designed. Its structure and working principle were introduced, and the key components – such as the metering disc, seed cell, and seed-protecting plate – were theoretically analyzed and designed. By adopting a seed pile stratification and centrifugal filling method, the issues of poor seed filling and the complexity of the seed-clearing structure under high-speed conditions were effectively resolved.

ii) Mathematical models were established by taking the rotating speed of the metering disc, the number of apertures, and the aperture diameter as factors, and analyzing their effects and interaction effects on normally sown. This result indicates that the working speed does not significantly affect the quality of feed index, demonstrating that the operating principle and structure of the metering device are well-suited for high-speed operations.

iii) By applying data analysis software to fit and optimize the experimental results, it was determined that when the rotating speed is 1729.01 rad/min, the number of apertures is 5, and the aperture diameter is 14 mm, the quality of feed index can reach up to 92.07%. The optimization results were validated through bench tests, confirming their reliability.

References

Anantachar M, Kumar PGV, Guruswamy T, 2010. Neural network prediction of performance parameters of an inclined plate seed metering device and its reverse mapping for the determination of optimum design and operational parameters. Comput Electron Agr 72:87-98. 1

Bu L, Kou Q, Sugirbay A, Chen J, Chen Y, 2024. An air-assisted mechanical hill-seeding device for foxtail millet (Setaria italica). J Agric Eng 55:1578.

Chen K, Liu X, He X, Wang X, Liu Y, Li W, 2022. Design and experiment of a wheel precision seed-metering device with cells for corn. Tehnički vjesnik 29:1741–1748.

Chen X, Zhang S, Dong J, Liu F, Jia X, Huang Y, 2024. Development of high-speed and precision metering device with gradient-feeding and control seed for soybean planting. J Agric Eng 55:1574.

Ding L, Yang L, Liu S, Yan B, He X, Zhang D, 2018. Design of air suction high speed precision maize seed metering device with assistant seed filling plate. T CSAE 34:1-11.

Ding Y, Li H, Gao J, Yu H, Wang Y, Feng D, 2023. Parameter optimization of finger clip plate garlic seed-metering device. Agriculture 13:2071.

Dong J, Gao X, Zheng Z, Zhao P, Bi Y, Huang Y, 2025. Design and testing of a posture-adjusting precision metering device for high-speed maize planting. Front Plant Sci 15:1458597.

Dong J, Zhang S, Zheng Z, Wu J, Huang Y, Gao X, 2024. Development of a novel perforated type precision metering device for efficient and cleaner production of maize. J Clean Prod 443:140928.

Gao X, Xie G, Li J, Shi G, Lai Q, Huang Y, 2023. Design and validation of a centrifugal variable-diameter pneumatic high-speed precision seed-metering device for maize. Biosyst Eng 227:161-181.

Gao X, Zhao P, Li J, Xu Y, Huang Y, Wang L, 2022. Design and

experiment of quantitative seed feeding wheel of air-assisted high-speed precision seed metering device. Agriculture 12:1951.

Guo J, Yang Y, Muhammad MS, Tan C, Wang L, Tang P, 2022. Design and simulation for seeding performance of high-speed inclined corn metering device based on discrete element method (DEM). Sci Rep 12:19415.

Han D, Zhang D, Jing H, Yang L, Cui T, Ding Y, et al., 2018. DEM-CFD coupling simulation and optimization of an inside-filling air-blowing maize precision seed-metering device. Comput Electron Agr 150:426–438.

Lei X, Liao Y, Liao Q, 2016. Simulation of seed motion in seed feeding device with DEM-CFD coupling approach for rapeseed and wheat. Comput Electron Agr 131:29–39.

Lei X, Liao Y, Zhang Q, Wang L, Liao Q, 2018. Numerical simulation of seed motion characteristics of distribution head for rapeseed and wheat. Comput Electron Agr 150:98-109.

Li C, Zhang D, Yang L, Cui T, He X, Li Z, et al., 2024a. Research on high-speed and clean production with a high-speed centrifugal maize precision seed metering device featuring variable hole insert numbers. Comput Electron Agr 227:109620.

Li C, Zhang D, Yang L, Cui T, He X, Li Z, et al., 2024b. Research on a centrifugal high-speed precision seed metering device for maize with airflow-assisted seed filling and cleaning. Comput Electron Agr 226:109434.

Li Y, Xing S, Li S, Liu L, Zhang X, et al., 2020. Seeding performance simulations and xperiments for a spoon-wheel type precision cottonseed-metering device based on edem. Mechanical Engineering Science 2:2615.

Li Z, Ren D, Huang J, Wu J, Duan D, Zhang T, Chen Y, 2025. Analysis of the seed filling performance influenced by maize seed shape, posture, and suction force. Biosyst Eng 256:104186.

Liao C, Chen J, Geng F, Tang X, 2022. Airflow basin structure numerical optimisation analysis and suction nozzle characteristics experimental study of vacuum-vibration tray precision seeder. J Agric Eng 53:1294.

Liu H, Guo L, Fu L, Tang S, 2015. Study on multi-size seed-metering device for vertical plate soybean precision planter. Int J Agr Biol Eng 8:1-8.

Ma C, Yi S, Tao G, Li Y, Liu H, 2024. Theoretical analysis and experiment of seed-picking mechanism of belt high-speed seed-guiding device for corn. J Agric Eng 55:1543.

Nikolay Z, Nikolay K, Gao X, Li W, Mi G, Huang Y, 2022. Design and testing of novel seed miss prevention system for single seed precision metering devices. Comput Electron Agr 198:107048.

Ospanova S, Aduov M, Kapov S, Orlyansky A, Volodya K, 2024. The results of experimental research of a rotor seed-metering unit for sowing non-free-flowing seeds. J Agric Eng 55:1556.

Shang Y, Zhou B, Yang J, Zhang S, 2024. Design and experiment of impeller seed guide device for rice internal suction hole direct seeding device. Sci Rep 14:13300.

Tang H, Xu C, Wang Z, Wang Q, Wang J, 2022. Optimized design, monitoring system development and experiment for a long-belt finger-clip precision corn seed metering device. Front Plant Sci 13:814747.

Tang H, Xu F, Guan T, Xu C, Wang J, 2023. Design and test of a pneumatic type of high-speed maize precision seed metering device. Comput Electron Agr 211:107997.

Wang J, Tang H, Guan R, Li X, Bai H, Tian L, 2017. Optimization design and experiment on clamping static and dynamic finger-spoon maize precision seed metering device. Nongye Jixie Xuebaoy 48:48–57.

Xie C, Yang L, He X, Cui T, Zhang D, Li H, et al., 2025. Maize precision seeding scheme based on multi-sensor information fusion. J Ind Inf Integr 43:100758.

Xiong D, Wu M, Xie W, Liu R, Luo H, 2021. Design and experimental study of the general mechanical pneumatic combined seed metering device. Appl Sci 11:7223.

Xu H, Liu W, Liu H, Liu Z, Zhang G, 2025. Design and performance test of a combined and adjustable precise rice seed metering device. Int J Agr Biol Eng 18:101–114.

Zhao P, Gao X, Su Y, Xu Y, Huang Y, 2024. Investigation of seeding performance of a novel high-speed precision seed metering device based on numerical simulation and high-speed camera. Comput Electron Agr 217:108563.

Received: 26 May 2025; Accepted: 2 March 2026.

Contributions: all authors made a substantive intellectual contribution, read and approved the final version of the manuscript and agreed to be accountable for all aspects of the work.

Conflict of interest: the authors declare no conflicts of interest.

Funding: this research was funded by the Jiangsu Province Modern Agricultural Machinery Equipment and Technology Demonstration Promotion Project, grant number NJ2025-03; the Funded by Basic Research Program of Jiangsu, grant number BK20252050; the China Postdoctoral Science Foundation, grant number 2025M772473.

Data Availability Statement: the data used in this study were self-tested and self-collected. As the control method designed in this paper is still being further improved, data cannot be shared at present.

Acknowledgments: the authors are grateful to anonymous reviewers for their comments.